

CHARACTERISTIC DEFECTS-CORROSION DAMAGE AND MECHANICAL BEHAVIOR OF DUAL PHASE REBAR

Ch. Apostolopoulos¹, Arg. Drakakaki^{1*}, Alk. Apostolopoulos², T. Matikas²,
A.I. Rudskoi³, G. Kodzhaspirov³

¹University of Patras, Panepistimioupolis Rion, 26500 Patras-Greece

²University of Ioannina, Ioannina, Greece

³Peter the Great St. Petersburg Polytechnic University, Polytehnicheskaya 29, St. Petersburg, 195251, Russia

*e-mail: drakakaki@mech.upatras.gr

Abstract. The demands for constructions with high mechanical performance, located in seismic areas, expressed through EC2 and EC8- part3, were importantly satisfied mainly with the use of Tempcore dual phase steel bars. High mechanical performance of dual phase steel comes from the combination of the mechanical properties of each individual phase. However, several times have been reported problems concerning their structural cohesion.

In the present study four different technical classes (DP) of reinforcing steel bars were used: B500c, B450c, B400c and B500b. SEM and EDX analyses were used, focusing not only on the internal defects regions of the materials (before and after corrosion), but also on the external areas affected by pitting corrosion. Moreover, in terms of the experimental procedure, mechanical tensile tests were conducted, on both corroded and non corroded reinforcing steel bar specimens and the pertinent results are analyzed.

The conclusion from the present study is that both internal and external defects constitute a major problem for constructions, by diminishing their mechanical performance and resulting in their premature failure.

1. Introduction

During the last years, extended disasters were reported after powerful earthquakes. These facts raise speculations concerning not only the structural integrity and the performance of the constructions, but also the sufficiency of the technical characteristics and demands of the high strength steel bars used. The demand for constructions with high mechanical performance in earthquake prone areas of the EU was expressed through Eurocode 2 [1], Eurocode8- part3 [2]. These regulations demanded the use of high mechanical performance steel (high strength and ductility) category c. This demand was satisfied with the adoption of Tempcore dual phase steel bars, which occupy an increasing market share and with the micro-alloyed steel bars as well.

As it is widely known, dual phase high performance steel, which is made of scrap metal, shows an external high strength zone (martensitic phase) and a softer core (ferrite-perlite phase). Beyond these two obvious phases, there is a transition zone called bainite phase. The high mechanical performance of dual phase steel comes from the combination of the mechanical properties of each individual phase, where the increased strength properties are credited to the presence of the outer martensitic zone, and the increased ductility to the ferrite-perlitic core. Due to the coexistence of the different phases, an assumption could be made, that the continuity and the coherence of the structure of the specific type of steel is taken for granted. However, this anticipation is not always satisfied, since given the variety of the phases, there are distinct areas

of different types of crystal structures and consequently different types of mechanical behavior on each phase of the material. Moreover, quite often, final products suffer from surface and internal defects, which deteriorate the final product quality. These defects occur at the early stages of the casting of the steel bars, as it was analyzed in study [7], which was presented at the 11th International Scientific and Technical Conference, which took place in Saint Petersburg in Russia on 2015. Similar information is given in studies [3-6].

Studies [8, 9] are related to internal micro cracks, micro voids and non-metallic sulfide compounds (MnS, FeS), which react selectively to the presence of chlorides (coastal environment) and contribute towards their fast and dangerous swelling.

Inclusions, voids, cracks and micro-cracks can be formed within steel microstructure during solidification of steel, as Thomas [3] refers. Sulfur and phosphorus are undesirable impurities in steel, since they may lead to low toughness, poor weld ability and so on. As it has been proved by various studies, such as [10], the size and the morphology of sulfides in steel may cause additional problems. Large sulfides usually result in poor mechanical properties, and non-spherical sulfides are responsible for certain anisotropic properties due to their non determined shape, resulting in the diminishment of the materials performance.

However, internal defects are not the only factor that affects the internal structure of steel. Another important and equally harmful factor is the surrounding environment. A typical example is the saline environment, which is rich in chlorides, that performs an intense action. There are various examples of European countries, which are located in coastal environment, that need to confront the intense erosive activity which usually begins in the form of pitting corrosion. Pitting corrosion is a localized degradation of the corrosion resistance of the metal, which initiates by the penetration of some aggressive anions, such as Cl⁻ ions, through ruptures found at discrete sites on the passivated film layer. It is a highly localized form of corrosive attack that leads to the loss of material. Study [11] refers that in some cases, if left to continue, then pitting may increase to full wall thickness perforation.

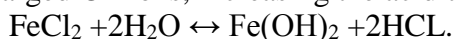
According to [12], pitting may act as an initiator of another, much localized corrosion like crevice corrosion, shielded by corrosion products and inter-granular corrosion at grain boundary region. It also acts as a local stress raiser to environmentally induced cracking viz. SCC (stress corrosion cracking) and HIC (hydrogen induced cracking). Pitting corrosion is one of the main causes of the performance deterioration and structural failures of industrial systems.

Once pitting has been initiated, the growth of the pits will depend on the charge difference of the electric field strength between the regions within and around the pits. Metal dissolution within the pits produces excessive charge. Negatively charged Cl⁻ ions migrate from the surrounding area towards the pit cavity to induce the corresponding neutralization. The rate of Cl⁻ migration (or pit propagation) depends on several factors such as pit shape, surface roughness and salt films concentration. Paul and Biswas [12] mention that the combination of all these factors results in a more aggressive pit environment than the critical chemistry needed to encourage pitting growth. After pitting initiation, growth is controlled by the following electrochemical reactions.

Anodic reactions inside the pit:

$\text{Fe} \leftrightarrow \text{Fe}_2 + 2\text{e}^-$ (dissolution of iron) [12]. The electrons given up by the anode (inner wall of the pit) flow to the cathode (passivated surface outside the pit) where they are discharged with the following cathodic reaction:

$\text{O}_2 + \text{H}_2\text{O} + 2\text{e}^- \leftrightarrow 2(\text{OH}^-)$ [12]. The effect of these reactions is that the electrolyte within the pit is enriched with the positively charged ions, in contrast to the surrounding electrolyte of the pit, which becomes negatively charged. The positively charged pit attracts the negatively charged Cl⁻ ions, increasing the acidity of the electrolyte according to the following reaction



The previous reaction produces HCl, which aggravates further dissolution of the metal,

producing more Fe^{++} within pit and hence excessive charge again by the above reaction. Consequently, the previously referred steps keep repeating, simulating pit growth to an autocatalytic process. Steel corrosion can be arisen from the exposure to corrosive media, such as sour gas or hydrogen sulfide (H_2S), carbon dioxide (CO_2) and free water. Frequently, relatively high operating temperatures and pressures get involved, which can further exacerbate the rate of corrosive attack. Furthermore, study [13] mentions that due to the possibility of the presence of a ‘cocktail’ of corrosive media, a simultaneous action of combined corrosion mechanisms may take place. The results of the experimental study, which was conducted by Apostolopoulos et al. [4], showed that for equal mass loss rates, due to corrosion process, among the embedded and the bare dual phase steel bar specimens, embedded specimens recorded higher mechanical degradation. This fact was associated with the higher surface damage which was observed due to pitting corrosion.

Various studies have been conducted by many researchers [5, 6, 7, 8, 14, 15, 16] on the detection of internal structural imperfections of the material and their development over time (under corrosion conditions). Avci et al. [17] in their study depict a sulfide area, as well as the surrounding dissolution mechanism of the material of the iron. This particular morphology, of protruding MnS at the center of a pit, is pretty common in the early stages of pit initiation and development. Notice also that MnS does not erode as fast as the surrounding Fe matrix during the initial stages of corrosion. The proposed mechanism of corrosion is depicted in Fig. 1. It is very likely that the adsorption of Cl^- ions in and around the strained regions of a MnS–Fe interface triggers the anodic dissolution of Fe^{2+} ions. It is important to reemphasize here that Cl^- ions are not involved in redox reactions, but catalyze the anodic processes by adsorbing on the surfaces around the MnS inclusions and by chasing away the conduction electrons of the strained matrix, which results in the anodic dissolution of iron from these regions as depicted in Fig. 1 [17].

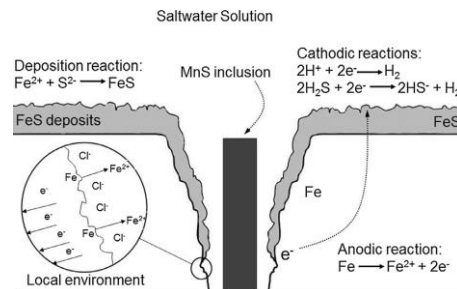


Fig. 1. Corrosion mechanisms surrounding a MnS inclusion: refer to [17] for details.

The study that was conducted by Negheimish et al. [18] is worth noticing as well. In the frames of the specific study manganese sulfide [MnS] inclusions in steel rebar are examined, exposed to simulated concrete pore solution to understand their role in passive film, corrosion and pit propagation behavior. The results showed that MnS inclusions adversely affected the nature of passive film and accelerated corrosion and pit formation. Results of studies [6-7] refer to frequently occurring defects, the majority of which firstly appear during the casting procedure. This fact has an impact on the mechanical performance and the reliability of steel bars, since in many cases sulfide and microvoid areas act as stress concentration points or motivate micro cracks formation during the loading, a fact that has been mentioned in study [19] as well. The average stress concentration inside the inclusion is higher for more rigid inclusions. The properties which have been defined for the interface govern the average stress concentration around soft inclusions, but the stress concentration around the inclusions with higher rigidity factor is related to the properties of the matrix. Investigation of the size effect of the inclusion on the level of the stress concentration reveals a critical size of the inclusion where the stress concentration does not increase with the growth of the inclusion for a given applied

load and boundary conditions. However, during the violent loading, recycles may cause coalescences of critical importance for the steel, due to their proximity, forcing a multiple cracking phenomenon. This phenomenon has also been described in [20]. Moreover, according to [4, 6, 7, 15], corrosive environment also causes not only surface damage assisted by pits, but also damage within the outer surface, due to sulfide existence on the martensite area. This fact results in the extension of the damage in depth. According to the same study, rapid depletion of the ductility, or even failure, may occur in high strength and ductility dual phase steel bars, due to the combination of interior and exterior damage phenomena under strong stresses.

The main purpose of this study is to describe and to evaluate the influence of corrosion on dual phase steel bars and to estimate the degradation of its mechanical properties and performance, which is the result of the cooperation of the internal and the external damage, under those hazardous circumstances. What is also analyzed is the fact that induced damage is not owed only to internal defects, but also to the detriments resulting from the prevailing environment conditions, which are responsible for the development of the external damage.

2. Experimental procedure

The materials used in the present study were four different technical classes (DP) of reinforced concrete steel bars, namely B500c, B450c, B400c and B500b, coming from European factories, which were produced by the same steel manufacturer using the “tempcore” method. The chemical composition, which is approximately the same for the four different steel bar categories, is presented in Table 1.

Table 1. Chemical composition of B500c, B450c, B400c and B500b steel bar categories.

	B500c, B450c, B400c, B500b
C, %	0.22
P, %	0.050
S, %	0.050
Cu, %	0.80
N, %	0.012

In Fig. 2 are shown representative optical micrographs of a DP-steel B500c ($\Phi 12$), produced in this work, that were etched revealing the martensitic skin, the transition zone and the ferritic -perlitic core, upon immersion in a Nital solution 2 %. In the microstructures shown in Fig. 2, the bright grains are the ferrite phase and the dark ones are the martensite. At their transition zone, bainite phase can be recognized. At the same time, SEM and EDX analyses were used for the analysis of the fracture surfaces, focusing not only on the internal defects regions of the materials (before and after corrosion), but also on the external areas affected by pitting corrosion. Moreover, in terms of the experimental procedure, mechanical tensile tests were conducted, on both corroded and non corroded reinforcing steel bar specimens. The pertinent results are analyzed.

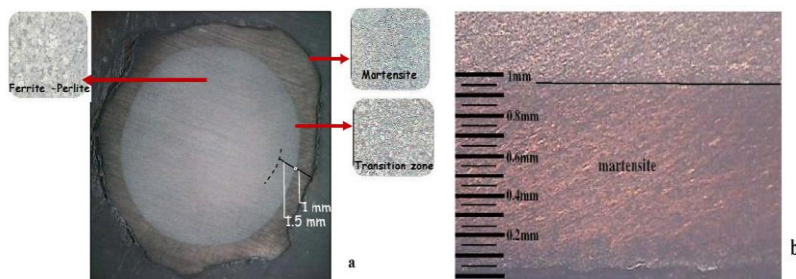


Fig. 2. Representative optical micrographs of a DP-steel B500c, etched, revealing the different phases discrimination, upon immersion in a Nital solution 2 %.

Half of the B500c specimens used have a 10mm diameter. The rest specimens have a 12 mm diameter and 510mm length each. All the steel specimens of $\Phi 10$ and $\Phi 12$ were taken from different sources. This process was followed not only for bare specimens but also for embedded, which were prepared in cylindrical shape with peripheral concrete cover equal to 10 mm, compressive strength equal to 20 MPa and C16/20 class of concrete.

As far as the rest three categories (B400c, B450c and B500b) are concerned, the specimens used had a nominal diameter of 16mm and 1m length. Besides these, two reference specimens, with 10 mm diameter, which belong in B500c steel bar category, were mechanically tested.

2.1. Artificial Corrosion and the Mechanical Tests of the specimens. The specimens used, (directly exposed to the corrosive medium) were inserted in a laboratory salt-spray exposure chamber, in accordance to the ASTM B117-94 [21] specification. The exposure of the bare and the embedded specimens to the corrosive medium was direct and was defined for the different periods of 15, 30, 45, 60, 75 and 90 days for the bare and of 30, 60 and 90 days for the embedded respectively.

The ASTM B117 [21] specification covers every aspect of the apparatus configuration, procedure and conditions required to create and maintain a salt spray (fog) testing environment. The selection of such a procedure for corroding the specimens, relies on the fact that the salt spray environment lies qualitatively closer to the natural coastal (rich in chlorides) conditions than any other accelerated laboratory corrosion test. In principle, the testing apparatus consists of a closed chamber in which a salted solution atomized by means of a nozzle, produces a corrosive environment of dense saline fog. The salt solution was prepared by dissolving 5 parts by mass of sodium chloride (NaCl) into 95 parts of distilled water (pH range 6.5–7.2). The temperature inside the salt spray chamber was maintained at 35 °C (+1.1–1.7) °C. The corrosion procedure was carried out at a cycle time of 3 hours resulting in 8 wet-dry cycles per day.

At each testing date specimens were removed from the salt spray chamber, washed with clean running water to remove any salt deposits from their surfaces and air-dried. The corrosion products were removed from the surface of the specimens by means of a wire brush, according to ASTM G1 specification [22]. The specimens were then weighted and the mass loss due to corrosion exposure was calculated with the use of equation (1):

$$\Delta m = [(m_o - m_c) / m_o] * 100 \%, \quad (1)$$

where, m_o is the mass of non-corroded specimens and m_c the reduced mass of the corroded specimen. Both reference specimens (before corrosion) and specimens exposed to corrosion for different periods were subjected to tensile mechanical tests.

The tensile tests were performed according to the ISO/FDIS 15630-1 specification [23], using a servo-hydraulic MTS 250KN machine with a constant elongation rate of 2 mm/min. Each bar was cut to the tensile testing length of 510 mm, according to the standard. The mechanical properties, yield strength R_p , ultimate strength R_m , and uniform elongation A_{gt} , were determined.

3. Results and Discussion

Results mainly refer to the most representative and significant cases of the mechanical behavior of the specimens, coming from the four different dual phase steel bar categories. A few specimens were additionally submitted to cross and longitudinal sections so as to properly formulate, after grinding and careful polishing, certain plates in the demanded geometry.

The preparation of the slide specimens for SEM analyses was performed as follows: Grinding and polishing of the samples were carried out on a Minimet TM grinder Polisher machine (Buehler Ltd.). After normal grinding of the sample surfaces with SiC paper, diamond and SiO₂ polishing compounds were used for producing stress free surfaces. Scanning electron microphotographs recorded with field emission scanning electron microscope (ZEISS, SUPRA

35VP) operating at 15 and 30 keV accelerating voltage. The microscope is equipped with backscattered electron detector and x-ray microanalysis system (QUANTA 200, BRUKER AXS) in order to get the appropriate information's from the surface structure of the samples.

Similar SEM-EDX analyses were performed on fracture surfaces (corroded and non-corroded), with the use of X rays, after rigorous polishing. For B500c dual phase steel bars, $\Phi 12$ diameter, the findings (before corrosion) revealed the existence of microcracks and microvoids in the material. These findings were detected locally and are characterized as internal defects of the materials. Moreover, through X rays diffusion, the appearance of pores was obvious at the external martensitic surface and at the same area high sulfide concentration was noticed. This fact increased the requirements for damage expansion at the inner area of the external surface (skin). Given the sensitivity of the sulfides to corrosion, in these areas, more attention is paid to items such as copper content, which are factors that should be attributed to the quality of the scrap metal used. From certain images of the specimens that were placed under treatment, was found that within 50 microns from the outer surface develops an area with elongated "dividing" undulations, which seems to obey on the shaping of the steel in steel bar, with Mn, Cu and Si (Figs. 3 and 4).

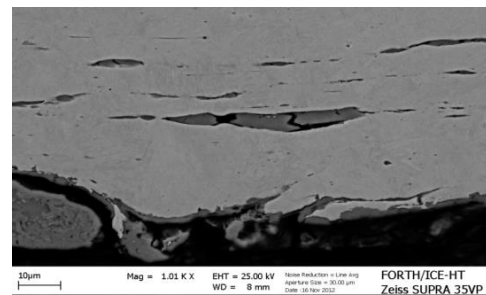
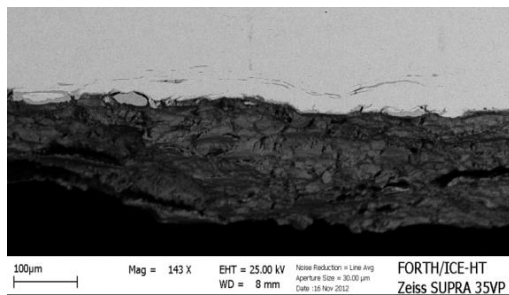


Fig. 3. Surface layer of 50 μm thickness, with elongated "dividing" undulations, rich in MnS, Si and Fe oxides.

Fig. 4. Surface layer of 50 μm thickness, with elongated "dividing" undulations, rich in MnS, Si and Fe oxides.

Such a phenomenon is considered to be quite common on the external surface, even before corrosion. Moreover, it should be noted that at these areas a native intergranular corrosion can be detected, even before the artificial corrosion of the specimens in the salt spray chamber. These phenomena, in combination with the extended sulfides (MnS, FeS) development in the outer zone of the material, constitute, without a doubt, a characteristic tendency of the material to corrosion (Fig. 5).

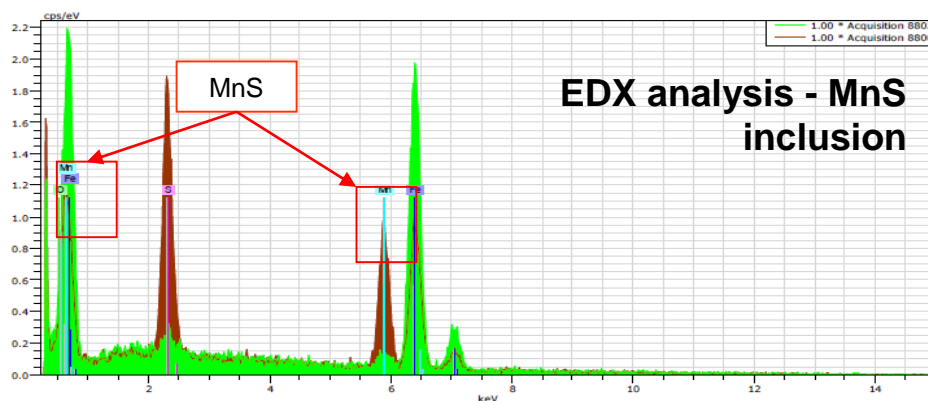


Fig. 5. Extended sulfide development in the outer area of the material.

Characteristic defects (oxides and sulfides), as well as intergranular corrosion phenomena, not only constitute very serious degradation factors for the material but they also have impact on its mechanical performance.

On non corroded steel bars B500c category, $\Phi 12$ diameter, which were subjected to tensile tests up to the neck appearance (before failure), several cross sectional areas at different depths were examined, via SEM optical processing. At those areas, several voids, inclusions and sulfides were revealed. Figure 6 shows a spot series (inclusions, sulfides) and voids which surround the granular groups and can affect the mechanical behavior of the limit load cases.

Figure 6 focuses on the martensitic area in 350 μm depth.

In Fig. 7 is presented an impressive microphotograph, where the grey spots are turning into polygonal patterns, each of which is surrounding grains groups.

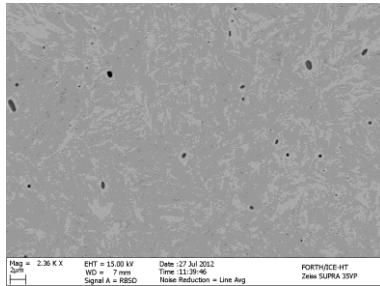


Fig. 6. Voids and inclusions in the martensitic zone.

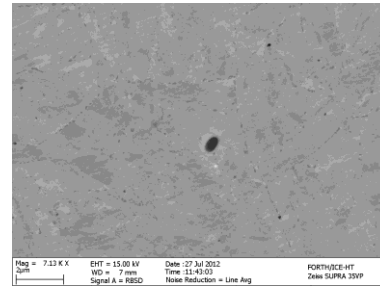


Fig. 7. Voids surrounding grains groups.

Figures 8 and 9 derive from EDX process, which shows the existence of either visible or not visible sulfides as well as the dispersed copper (Cu), which is possibly owed to the scrap provenance of the material.

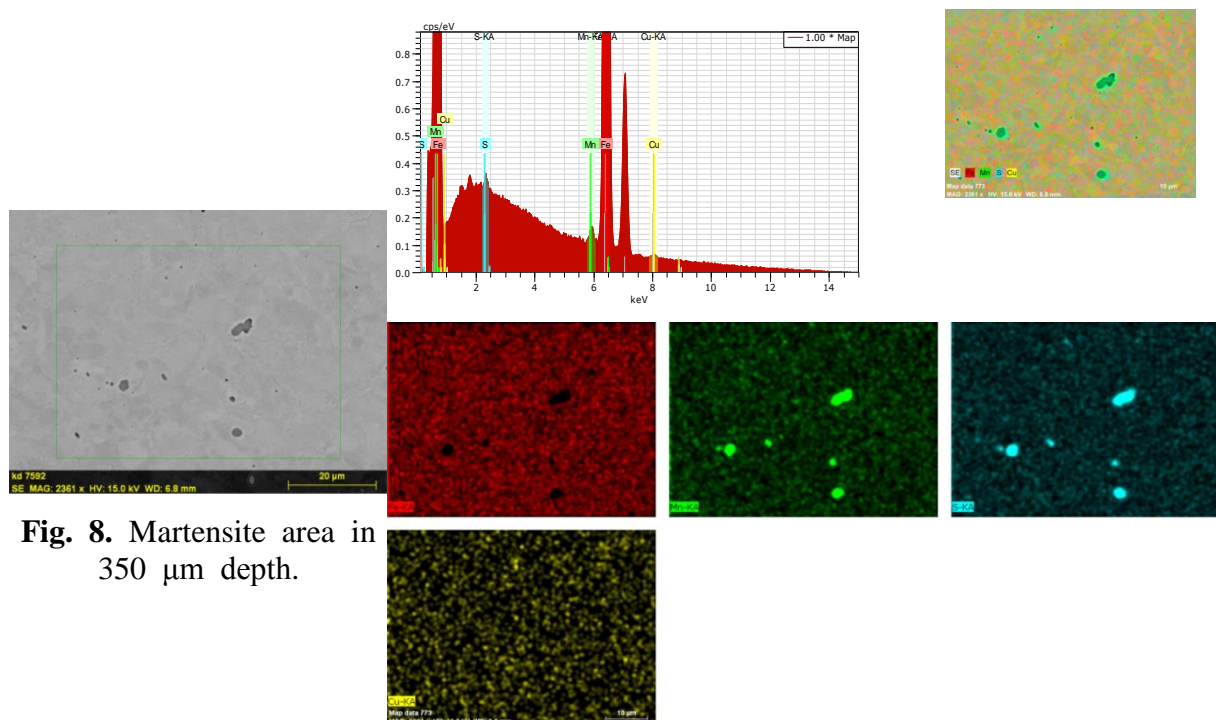


Fig. 8. Martensite area in 350 μm depth.

Fig. 9. Stoichiometry in 350 μm depth.

Figure 10, which has been taken from [6] study that processes on the same rebar group, presents a SEM analysis of a longitudinal cut in the fracture region in a non - corroded B450C specimen after tensile test.

Certain results of the present experimental procedure, which were published in [6] and constitute a part of an ongoing study conducted by prof. Apostolopoulos prove that both defects

and voids have been obviously extended and oriented to the direction of the (growing) external applied load. The deviation from horizontality at 13-15 degrees is caused by the development of shear stresses (shear deformation is dominant) in the failure location of the specimen. Furthermore, at those areas, voids were more frequent. Certain of the voids, located near the fracture surface, were elongated in the tensile direction. The development of the particularly intense deformations in the fractured area clearly contributes to the elongation and coalescence of interior holes. On the fracture surfaces porosity and inclusions were recorded. In general, these two types of defects appear to have a significant impact on failure, since throughout the entire length they have their negative imprint. This information has already been mentioned in [6].

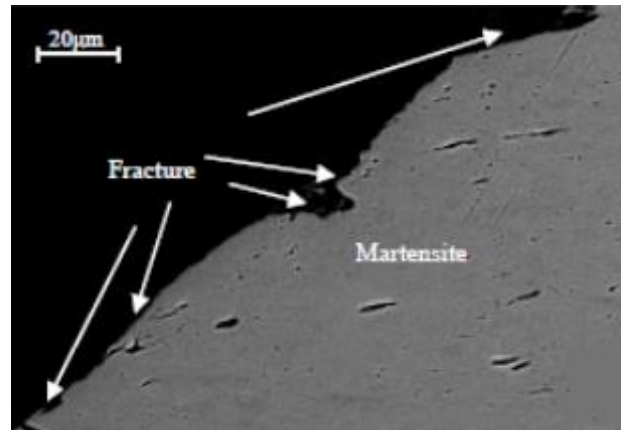


Fig. 10. Fracture surface (longitudinal cross section) of a non corroded specimen B450c [6].

Figure 11 is taken from $\Phi 10$ specimen, in 770 μm depth, where the martensitic zone ends and the transition zone (bainite) begins. At the area where the three metallurgical phases (martensite, ferrite and perlite) coexist, voids and sulfides detection was confirmed. Similar findings were recorded in ferritic-perlitic area, at 2500 μm depth.

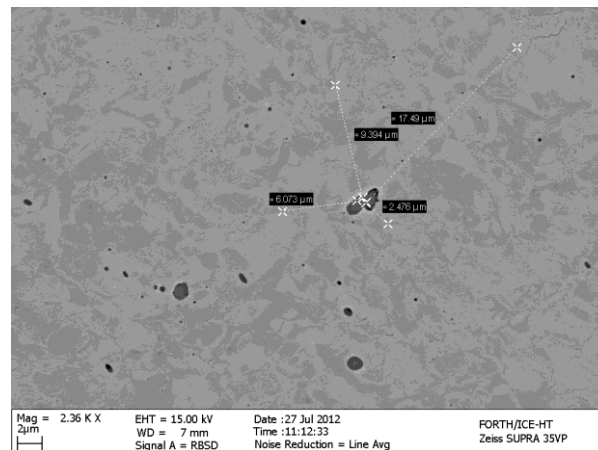


Fig. 11. Intense presence of sulfides on the transition zone of a $\Phi 10$ specimen, in 770 μm depth.

Certain important findings concerning a longitudinal section of a non corroded B500c steel bar, $\Phi 10$ diameter are presented in Figs. 12a-c. The elongated inclusion (2300 μm length) which has been detected in the martensite-bainite interface (transition zone) is characterized by the intense presence of sulfides, oxides and voids, which from one point of view have no “mechanical performance”. On the other hand, it constitutes a region, which in presence of chloride ions is responsible for the destruction of the surrounding iron (Fe).

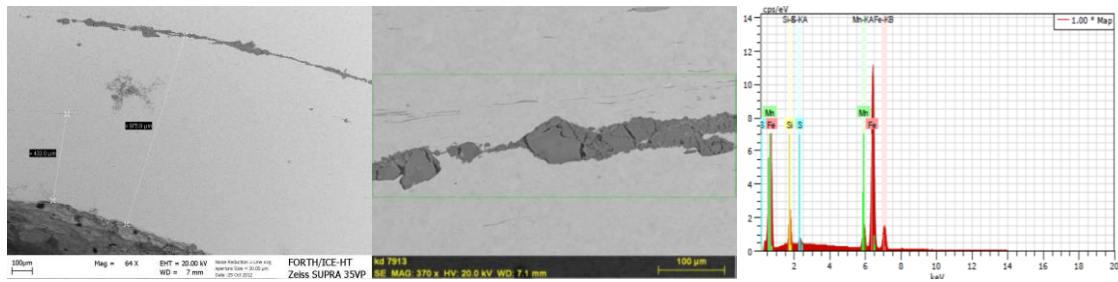


Fig. 12. (a). An important finding on a longitudinal section of a non corroded B500c steel bar with 10 mm diameter, (b). Intense presence of sulfides, (c). FeS and MnS identification through EDX image processing.

Moreover, it is believed that the coexistence and the continuance of the material between the phases of the martensite and the core (interface limits) is sustained and coherent. However, from a metallurgical point of view, it is not true. Reality lies in the fact that the interface is not coherent in the boundaries, between the ferritic-perlitic zones, as it is a region of different crystal types with subsequently different mechanical properties. Figs. 12a-b, 13, 14, and 15 confirm this view. Under laboratory investigation on the mechanical behavior of the transition zone, a $\Phi 8$ B500c steel bar sample was recorded (the martensitic percentage was calculated at 24 %), after the imposition of eccentric compressive load pointed at the martensitic skin of a cross section on the kinematic behavior of the gauge. In reference to this fact, Figs 13, 14, and 15 present various point of views, such as the surface of the slip area and the lower level of the core. Rupture of the two phases and slide lines can also be observed.

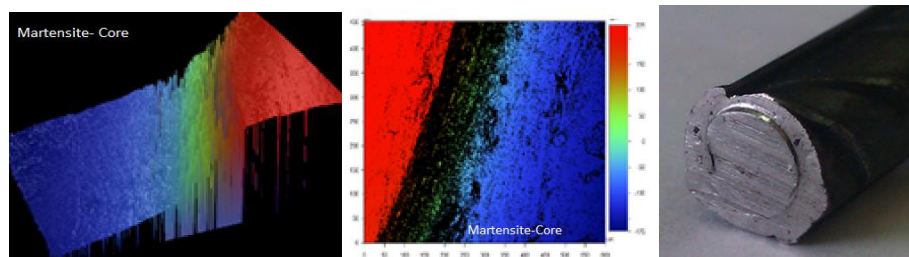


Fig. 13. Veeco Device shows the detachment between Martensite–Core (about 400 μm).

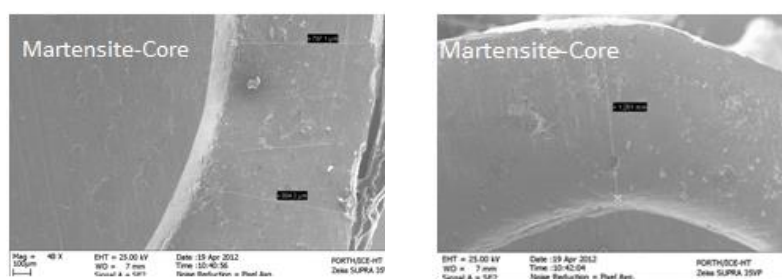


Fig. 14. (a, b). The area where the external martensitic skin slips towards the core is indicative.

Further cross sections and focus (via EDX analysis) on the interface of the martensite and the transition zone (bainite) revealed silicon and iron oxides, as well as sulfides derived from the production process of the material. The extension of these findings, constitute possible threats for steel mechanical degradation. Mechanical degradation is owed to the fact that the previously referred oxides and sulfides cannot receive any load and for this reason they constitute potential sites for stress concentration development. This fact has been described in recent studies [10, 24, 25, 26].

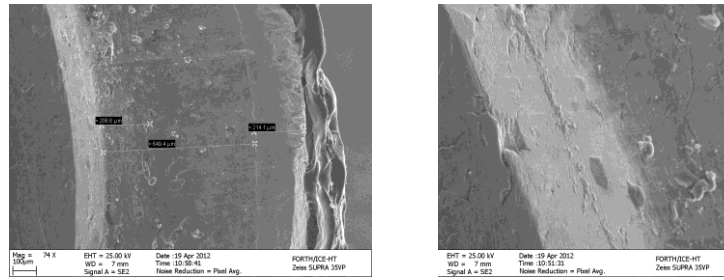


Fig. 15. (a, b). The presence of concentric cracks peripheral to the degraded part of the martensitic skin.

It is well known that many researchers have reported the ductile failure mode of dual phase steels with major reports in studies [27, 28]. Studies [29, 30] attributed the failure to void formations resulting from the fracture of martensite elements and the detachment from the interface of the martensitic and ferritic-perlitic zone. Steinbrunner and Krauss [31] conducted a micro mechanical study so as to investigate the process of failure in dual phase steels and observed three mechanisms of void formation, namely, the detachment of interfaces, the fracture of martensite and the individual withdrawal of the martensite. Kang and Kwon [32] studied the fracture behavior of steel structure (in medium carbon steels) and observed that the ferrite-martensite interface decohesion was the predominant mode of the void nucleation and growth, where martensite structure was the lath type. Nam and Bae [16] showed that the overwhelming of the reports show that most of the voids that lead to fracture, were formed in the core- martensite interface, despite the initially cracked martensite. Ahmed et al. [8] mention 3 ways of void formation in grains: martensite cracking, detachment of the ferrite-martensite interface and detachment of the interface. They associate the failure mode with the percentage of martensite V_m content, the void formation results in detachments on the ferrite-martensite interface, while the other two mechanisms appear in higher rates of martensite (V_m more than 32 %). As far as the degradation of B500c steel bar category is concerned, it is thought to be owed to the detachment noticed between the different phases, instigated by the existence of the defects.

For the investigation of the mechanical behavior of the $\Phi 10$ B500c non-corroded specimens, five tensile tests were conducted, according to the standard, in a servo hydraulic MTS-100kN test system. The cross head speed of the automatic controller of the machine was 2mm/min and the tests took place at room temperature. During the most of these tensile loadings, a “knee” was observed at the elastic region. At the same time, elastic modulus reduction was recorded. A typical example is illustrated in Fig. 16, where the gradually deteriorating response of the material after corrosion is presented.

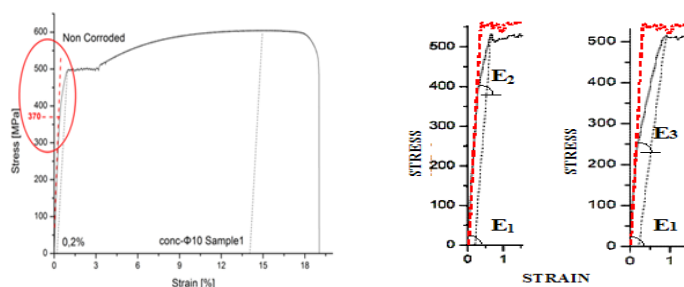


Fig. 16. Stress-strain curve of non-corroded specimen, $\Phi 10$, B500c category, with the appearance of a “knee”, in comparison with a corresponding corroded specimen.

The initial Young’s modulus E_1 , appears to take different values E_2 and E_3 , in each case (non corroded and corroded respectively), in respect to the loads which are gradually imposed to the material. As a result, the relevant value of yield strength point corresponds to an increased strain.

The occurrence of a "knee" in the elastic region of the reference specimens, led to further tests. The tensile tests of the non-corroded (reference) rod B500c $\Phi 10$, were performed until the necking initialization. Afterwards, several cross sections of 10mm each were cut successively along the bar's length. After numbering the samples, as shown in Fig. 17 and Fig. 18a, they were tested with the non-destructive method of ultrasound C-Scan, see Fig. 18b.

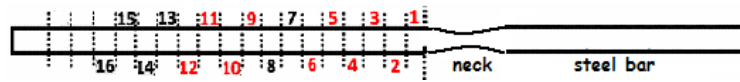


Fig. 17. Sample mapping.

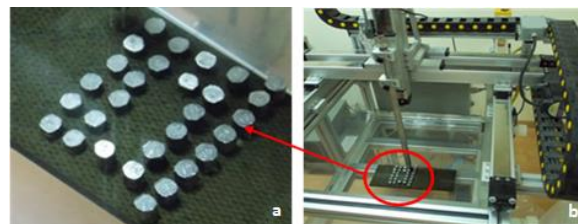


Fig. 18. Ultrasound inspection of samples.

Ultrasound examination was performed so as to detect and evaluate any internal discontinuities in the structure of the bar. The examination showed that the samples with numbers 1-6, 9-12 demonstrated a structural defect in the interface of martensitic and ferritoperlitic cortex, as shown in Fig. 19.

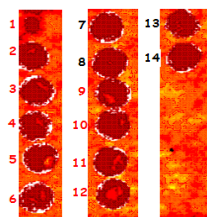


Fig. 19. Ultrasonic C-scan results.

However, the occurrence of "knee" in the elastic region along with the results (qualitative nature) of ultrasound process raised serious "hinds" regarding the non-consistent bonding of the martensitic cortex and the core, which led to further investigation. So, as to eliminate the possibility of structural defect in ferritic perlitic core of B500c, three mechanical tests were performed in the non-corroded specimens that had previously been lathed till they reached a 4 mm diameter, a point at which only the core remained. At this point, the results would allow us to know if there is an integral or an imperfect adhesion between the bainite and martensite phases. Figure 20 depicts a lathed specimen and Figure 21 presents its respective stress-strain diagram after a tensile test. In none of the three diagrams of the lathed specimens, did a "knee" occur in the elastic region.



Fig. 20. Lathed specimen till core remains.

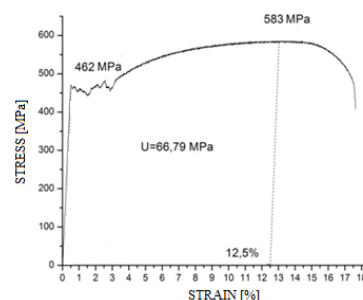


Fig. 21. A respective stress-strain diagram after a tensile test.

Excluding structural defect in the core of the material, the interest was focused on the examination of the fracture surface on the interface of the martensitic skin and the core, using Scanning Electron Micrographs analyses. Figures 22a,b clearly show a localized detachment in the interface of the martensite and the internal core of the pre-corroded material.

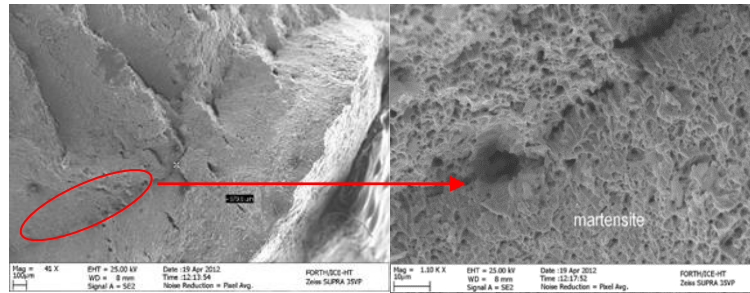


Fig. 22. (a, b). A detachment of the corroded martensitic skin can satisfactorily explain the formation of the "knee" in the elastic region. Focus on the boundary between the martensite and the core of the cross section.

In Fig. 22, the crack is located in a distance of approximately 700 μm from the external surface of the steel bar. This distance coincides with the average thickness of the martensitic cortex in dual-phase steel B500c, with a nominal 10 mm diameter. Taking these results into account, it can be suggested that the mechanical performance of certain series of steel specimens was not reliable.

Further tensile tests were conducted as well. Results given from B400c category, $\Phi 16$ (with a nominal 16 mm diameter), dual phase steel bars also show local irregularities close to the yield stress point and in the elastoplastic area. It should be noted that for the specific category, martensite constitutes the 27.50 % of the cross sectional area.

Conclusively, it appears that mechanisms like debonding and decohesion may initiate in several locations and in some of them lead to local detachment of the two metallurgical phases (Fig. 22).

These findings constituted the trigger for further investigation and several additional tensile tests as well. Within one of these tests in a non-corroded (reference) B500c $\Phi 10$ specimen, ultrasonic examination was performed, so as to detect and evaluate any internal discontinuities in the structure of the bar (Figs. 17, 18 and 19). The examination results showed that the areas located closer to the "neck" formation presented more structural defects in the interface of martensitic and ferritoperlitic cortex.

Similar bilinear behavior was also performed by the $\Phi 12$, B500c dual phase steel bar specimen series, which was elastoplastically loaded up to a 3 % deformation, during both loading and unloading (Fig. 23).

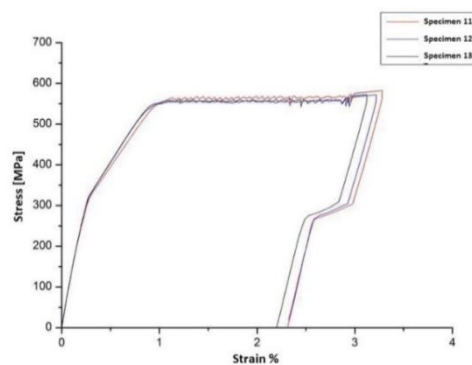


Fig. 23. Stress-strain curves for $\Phi 12$ non-corroded specimens, during tensile tests and unloading, with the "knee" appearance in both loadings.

Through the “knees” appearance, which resulted from the loads, a drop in the elasticity modulus was observed as well. This drop was in respect with the gradually imposed loads. It can be easily noticed that the strain corresponding to the yield point, appears particularly increased until the threshold of the yield strength of the material. The “knee” formation is probably owed to the production mode of the material.

During the tensile tests that were performed on corroded specimens, similar things were recorded as well. Figure 24 presents the stress-strain test of a corroded specimen, where the “knee” appearance is obvious. The gradual decline of the recorded stress, under which the “knee” formation occurs, appears to be associated with the degree of corrosion of the material. This phenomenon may be attributed to the corrosive agent that is responsible for both the gradual “softening” of the martensitic zone, due to the ageing that corrosion provokes, and for the development of pitting corrosion on the surface, which increases with regard to the degree of corrosion. The synergy of these two functions seems to be acting as a factor for further degradation of the material, given the fact that damage appears to be constantly spreading.

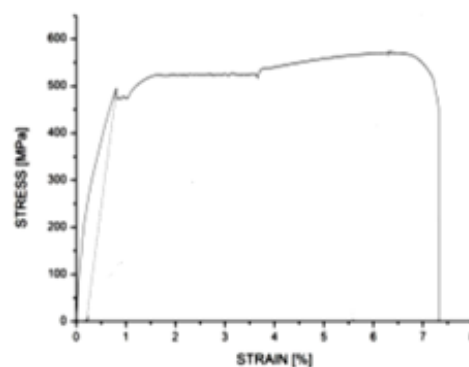


Fig. 24. Stress-strain curve for a $\Phi 12$ specimen, after 45 days of corrosion, during tensile test, with the “knee” appearance.

A worth-referring study, which deals with the “knee” appearance and the local detachment of the martensitic zone, is [33], from Masafumi Azuma. In that study, an effort was made to examine the response of each phase (martensite, ferritic-perlitic) to the loading imposed. According to the noticed behavior, martensite particles and ferrite grains present different strains even though the strain given is the same. To be more precise, strain in the martensite phase is much lower than the one in ferrite, although martensite particles deform plastically. It appears that the wide diversification is related to the shape and the distribution of the martensite particles in the ferrite matrix. A typical example is the low strain expressed by the ferrite grains, which are surrounded by the particles that comes in contrast with the high deformation of the isolated ferrite grains. The equiaxed martensite particles record lower deformation. According to [33], the strains are averaged at each strain.

The four more characteristic types of void formations are presented in Fig. 25:

- void initiated by cracking of a martensite particle,
- void initiation by decohesion at the interface between ferrite and martensite and coalescence of two voids formed at the end of martensite particles,
- void initiation by decohesion at the interface between ferrite and martensite and growth of a void formed at the end of a martensite particle and
- void formation by decohesion at the ferrite/ferrite grain boundary.

Through this depiction, it can be easily understood that the interaction among the existing internal and external defects is not a rare phenomenon, on the contrary, it is usually inevitable. This interaction is considered to be responsible for many failure scenaria of the material, as it can also be proved by the laws of Applied Fracture Mechanics.

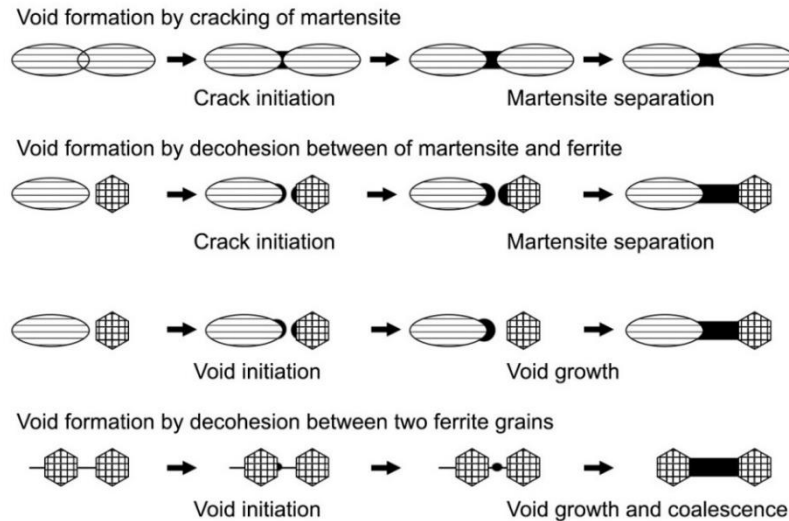


Fig. 25. Illustration of the four more characteristic types of void formation mechanisms between martensite particles in dual phase steels [33].

Namely, pitting, chloride and sulfide presence on the steel bars is considered to be very critical, since their interaction and their simultaneous action results in notches or cavities formation, or even in combined pitting. This interaction increases with corrosion exposure, leading to the initiation of corrosion paths formation (Fig. 26). Moreover, due to the increasing imposed deformation, there is a critical point at which crack growth and strain cannot continue. This is the point at which the hardening capacity is exhausted and final failure takes place.

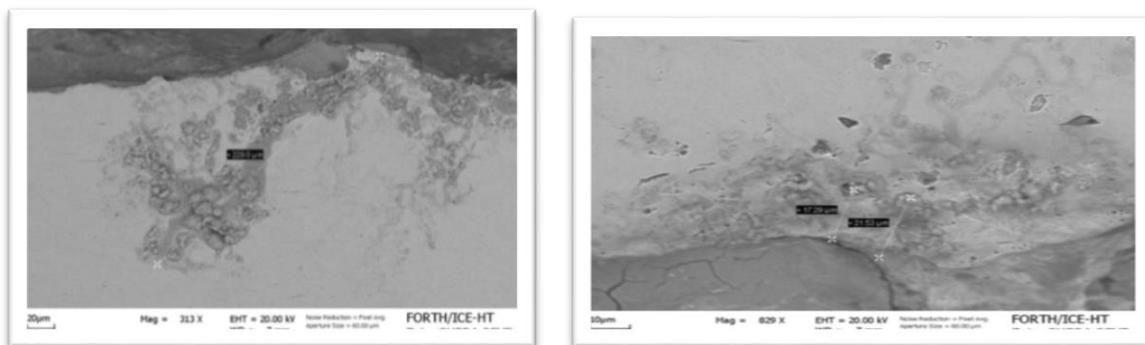


Fig. 26. Formation of corrosion paths.

Elaborating the external surface of dual phase steel bar and more specifically the quantification of the artificial corrosion damage, various measurements needed to be taken concerning not only the conventional term of mean mass loss, but also the mean and the maximum pit depth, as well as the mean and the maximum pit area.

For this reason, two specimen series (B500c, $\Phi 12$, 510 mm length, dual phase steel bar category) were prepared. In the first specimen group 18 bare specimens were included. In the second group 12 embedded specimens were included. The latter were constructed in cylindrical shape, with peripheral concrete cover 10 mm and C16/20 class of cement. Three specimens of each group were used as reference- non corroded cases. All the rest were inserted in the salt spray chamber for different exposure periods. For each exposure period, three specimens of each group were examined. Bare specimens were organized to 6 exposure periods (0, 15, 30, 60, 75, 90 days) and the embedded ones were organized to 4 exposure periods (30, 60, 90 days). After the completion of each predetermined period, the specimens were exported from the chamber and they were cleaned according to the pertinent standards. Mass loss was measured

for each specimen, and all the steel surfaces were meticulously examined, considering pitting corrosion, before the execution of the tensile tests. The results concerning mass loss and pitting measurements as well as the mechanical properties, or in other words the quantification of the artificial damage of both bare and embedded B500c steel bar categories $\Phi 12$ diameter, are presented in Tables 2,3.

Mass loss of bare steel bar specimens, constantly increases up to 12.48 % for a corrosion duration up to 90 days. Maximum pit depths values increase as well. On the contrary, pitting areas do not vary significantly. It is worth referring that pitting measurements in bare specimens demonstrate a uniform type of corrosion, in contrast to the corresponding results for the embedded case, where pitting corrosion is the dominant.

It should also be explained that for pit depth measurements, what was taken into consideration was the deduction between the initiation and the ending point of each pit, as well as the uniform reduction of the nominal diameter, which is owed to uniform corrosion. Consequently, a pit depth measurement in the present study equals to the sum of those two lengths.

Table 2. Pitting measurements and mechanical properties on embedded specimens, B500c category, $\Phi 12$ steel bar diameter, C16/20 type of concrete.

Exposure Time, Days	Mass Loss, %	Pitting measurements				Mechanical properties			
		Mean Pit Depth, μm	Max Pit Depth, μm	Mean Pit Area, mm^2	Max Pit Area, mm^2	(Rp), MPa	(Rm), MPa	Agt, %	(U), MPa
0	0	-	-	-	-	561,43	654,13	9.36	58.63
30	0.48	143	230	0.899	3.244	558.53	651.92	9.24	55.82
60	0.50	176	303	0.837	3.274	557, 41	650,08	8.74	52.50
90	0.65	172	393	0.919	3.448	556.90	647,90	8.35	50.12

Table 3. Pitting measurements and mechanical properties of bare steel bars B500c category, $\Phi 12$ diameter.

Exposure Time, Days	Mass Loss, %	Pitting measurements				Mechanical properties			
		Mean Pit Depth, μm	Max Pit Depth, μm	Mean Pit Area, mm^2	Max Pit Area, mm^2	(Rp), MPa	(Rm), MPa	Agt, %	(U), MPa
0	0	-	-	-	-	561.43	654.13	9.36	58.63
15	2.53	213	275	0.924	1.971	537.64	635.49	8.23	51.36
30	6.69	283	400	1.155	2.239	506.61	595.62	7.14	38.65
60	9.47	285	365	1.278	2.472	490.53	572.78	6.08	34.17
75	11.42	321	525	1.3635	3.04	467.80	548.11	5.54	29.48
90	12.48	350	548	1.18	2.209	453.29	530.99	4.85	25.17

On the contrary, mass loss of embedded steel bars, does not significantly vary between 30 and 60 days of corrosion (0.48 %-0.50 %). Something similar happens to the maximum areas affected by this factor as well. However, pitting maximum depth is steadily increasing. Maximum pit depth is equal to 393 μm for 0.65 % mass loss of the embedded specimens, while the same pit depth is reported for more than 10 % mass loss of the bare specimens. This fact confirms the assessment for pitting corrosion on the embedded specimens.

Moreover, certain further conclusions were made concerning pitting development: This particular behavior is associated with both the proximal pitting fusion phenomena and their further development see: Figs. 27a,b. Certain brief conclusions are given below:

- It is a common phenomenon for two close pits to extend to a larger one.
- Another case is the appearance of a localized damage due to concentrated pits along with localized corrosion
 - There are different shapes of pits, such as shallow and extended, or deep and narrow with steep pit walls, or even pits that contain inner pits.
 - Usually, the pit is located on the base of the rib, where a higher stress concentration will occur during loading.

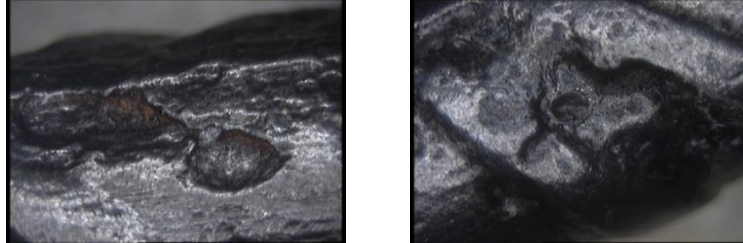


Fig. 27. (a, b). Various pitting shapes, (shallow, deep, sharp) constitute possible stress concentration positions.

Figure 28 graphically presents the change of the pitting factor (max pit depth/ mean pit depth) in reference to the mass loss, in red color for the embedded specimens and in blue color for the bare specimens, until 90 days of corrosion. It can be concluded that for mass loss about 0.65 % maximum pit depth value is about 400 μ m for embedded specimens. The same diagram shows that for mass loss lower than 0.50 %, pitting factor value is about 1.60. The same pitting factor value corresponds to 12 % mass loss for the bare specimens.

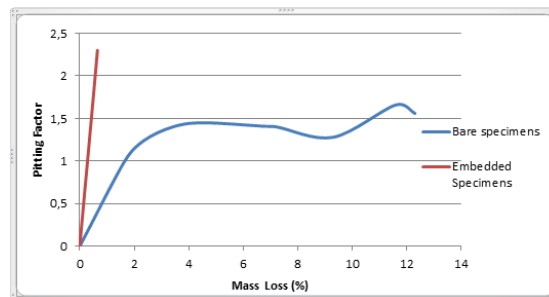


Fig. 28. Change of the pitting factor of the B500c, Φ 12, bare and embedded specimens in reference to mass loss (%).

On the other hand, for bare specimens it can be concluded that for mass loss about 2.5 %, pitting factor values range from 1.20 to 1.30. For mass loss about 10 % a range from 1.30 to 1.40 is recorded, while for mass loss about 12.50 % the values increase to a range from 1.35 to 1.60.

Conclusively, pitting factor values, which were taken from embedded specimens with low mass loss percentages (about 0.65 %) can depict in a very realistic way the corrosion effect on steel. Through these results, the importance of the external pitting factor on a critical failure mechanism is obvious, revealing the urgency of thorough study of its initiation and expansion.

Finally, SEM and EDX analyses, which revealed a gradual reduction of the adhesion between the two phases due to their imminent separation, strengthened our thoughts: see Figs. 29a,b.

The multiple responses of the phases of the material are owed to the differences between the metallurgical structures and the different strain hardening and strain rate sensitivity. The combined damage on the martensitic phase, due to corrosion factor, which was aided by external pits and internal defects close to the surface, is depicted in Fig. 30. Finally, in Fig. 31

is given a dual phase steel bar model, coming from Finite Element Analysis, using ANSYS Code, in reference conditions (Fig. 31a) and in corrosion conditions after pitting affection (Fig. 31b).

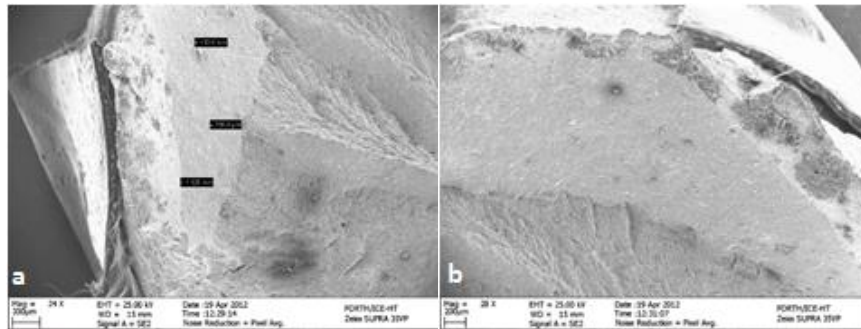


Fig. 29. (a, b) SEM-EDX analyses on the fracture surface of a specimen, after tensile loading.

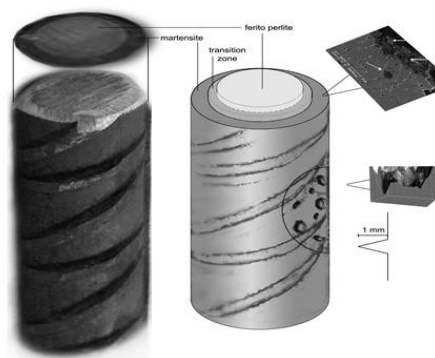


Fig. 30. Depiction of the internal and the external damage mechanism developed on dual phase steel bars after corrosion

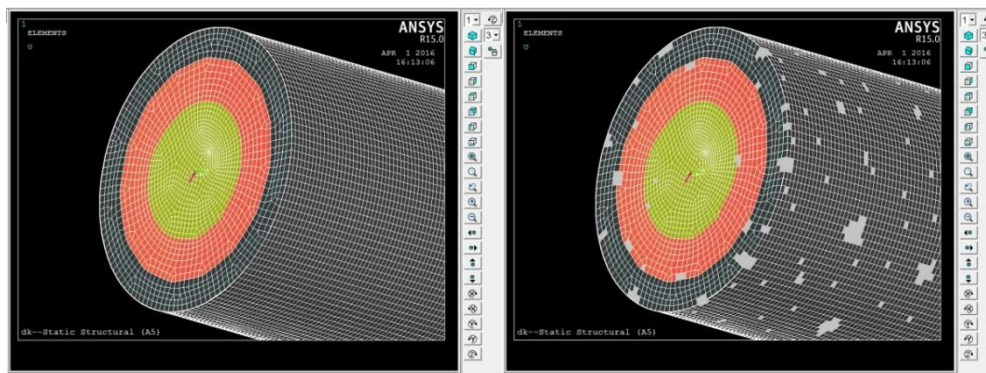


Fig. 31. Depiction of a finite element model (a) in reference conditions and (b) after corrosion affection.

The phases of the steel bar are discrete (martensite, transition zone and the core) and are presented in different colors. Given the figures, it is also easy to understand that the major damage on the corroded steel bar is located on the martensite layer and is not only a simple pitting result, but also the result of the combined action between pits and existing defects and their deterioration due to the harsh conditions, which quite often results in a coalescence among them. Last but not least, intense damage can also be noticed on the interface of the phases, resulting in their separation due to the loss of their adhesion. The source of this kind of damage is the existence of voids and sulfides and their swelling under corrosion conditions. The finite element model presented in Fig. 31 constitutes the first procedure of an ongoing study, which

tends to analyze the mechanical behavior of the dual phase steel bars, under defects and pitting affection. At this point it should be mentioned that external damage, caused by pitting corrosion, can be estimated by measuring the number of pits per unit area and by extended study of the surface, using optical instruments. On the contrary, for the estimation of the internal imperfections and defects, several intersections should take place in order to collect the data demanded to approach the real situation.

4. Conclusions

Making an effort to conclude the previously referred findings, what can be pointed out is that structural problems coming from the production process is a frequent phenomenon for dual phase steel bars, which is mainly related to microcracks, microvoids and sulfides presence.

- Pitting presence, which is owed to the various aggressive factors that exist in any corrosive environment, results in the damage deterioration both superficially and deeply
- During stress, sulfide areas and microvoids, may act as stress concentrating factors for the various dual phase steel bar categories, affecting not only their ductility, but also their strength, which is a factor that makes them occasionally unreliable.
- Moreover, phenomena like “knee” formation in the elastic region of the specimens, in combination with the corrosion level, constitute an important diminishing factor of dual phase steel bars, as far as their strength is concerned.
- The combination of internal and external defects on dual phase steel makes it a material characterized by an unpredictable mechanical behavior and this is because due to the coalescence of the defects, mechanical performance is diminished, resulting in the premature failure of the material.

Acknowledgments

It should be referred that certain of the experimental results presented in the current study, constitute a part of our work for the European program RUSTEEL.

References

- [1] *Eurocode 2, Design of concrete structures, European Committee for Standardization* (Brussels, Belgium, 2004).
- [2] *Eurocode 8, Design of structures for earthquake resistance, European Committee for Standardization* (Brussels, Belgium, 2004).
- [3] G. Thomas, In: *XXIV National Steelmaking Symposium* (Morelia, Mich, Mexico, 2003), Vol. 26-28, p. 138.
- [4] C.A. Apostolopoulos, S. Demis, V.G.Papadakis // *Construction and Building Materials* **38** (2013) 139.
- [5] C.A. Apostolopoulos, T. Matikas, G. Kodzhaspirov, G. Diamantogiannis, A. Apostolopoulos, In: *10th International Conference "Advanced Metallic Materials and Technology"* (Saint Petersburg, Russia, 2013).
- [6] C.A. Apostolopoulos, G. Diamantogiannis, A.C. Apostolopoulos // *Journal of Materials in Civil Engineering* **28** (2015) 2.
- [7] C.A. Apostolopoulos, A. Drakakaki, G. Kodzhaspirov, In: *11th International Scientific and Technical Conference* (Saint Petersburg, Russia, 2015).
- [8] E. Ahmad, T. Manzoon, Ali Kanwar Liaqat, J.I. Akhter// *ASM International* **9** (2000) 306.
- [9] C.A. Apostolopoulos, C.A. Rodopoulos // *International Journal of Structural Integrity* **1** (2010) 1.
- [10] Z. Liu, Y. Kobayashi, M. Kuwabara, K. Nagai // *Materials Transactions* **48** (2007) 12.
- [11] L.L. Shreir, R.A. Jarman, G.T. Burnstein, *Corrosion: Metal/Environment Reactions* (Butterworth -Heinemann, Elsevier, 1994).

- [12] S. Paul, I. Biswas // *Journal of Innovations in Corrosion and Materials Science* **5** (2015) 10.
- [13] P. Roffley, E.H. Davies // *Engineering Failure Analysis* **44** (2014) 148.
- [14] C.A. Apostolopoulos, G. Diamantogiannis, G.E. Kodzhaspirov, *Nanotechnologies of Functional Materials* (Saint Petersburg, Russia, 2012).
- [15] C.A. Apostolopoulos, G. Diamantogiannis // *Applied Mechanical Engineering* **1** (2012) 5.
- [16] W.J. Nam, C.M. Bae // *Journal of Material Science* **34** (1999) 5661.
- [17] R. Avci, B.H. Davis, M.L. Wolfenden, I.B. Beech, K. Lucas, D. Paul // *Corrosion Science* **76** (2013) 267.
- [18] A.A. Negheimish, A. Alhozaimy, R.R. Hussain, R. Al-Zaid, J.K. Singh, D.D.N. Singh // *NACE International* **70** (2014) 1.
- [19] L. Zhang, B.G. Thomas, In: *XXIV National Steelmaking Symposium* (Morelia, Mich, Mexico, 2003).
- [20] P. Juvonen, *Effects of non-metallic inclusions on fatigue properties of calcium treated steels*. PhD Dissertation (Helsinki University of Technology, Espoo, Finland, 2004).
- [21] *ASTM B 117-94, Standard practice for operating salt (fog) testing apparatus, Section 3: Metal test methods and analytical procedures* (West Conshohocken, Philadelphia, USA, 1995).
- [22] *ASTM G1, Standard practice for preparing, cleaning and evaluating corrosion test specimens* (2011).
- [23] *ISO/FDIS 15630-1, International Standard. Steel for the reinforcement and prestressing of concrete-test methods. Part 1: Reinforcing bars, wire rod and wire* (Geneva, Switzerland, 2002).
- [24] A. Belyakov, Y. Kimura, K. Tsuzaki // *Acta Materialia* **54** (2006) 2521.
- [25] A.W. Gjonnes, *Effect of Sulfide Inclusions in Austenitic Stainless Steel on the Initiation of Pitting in Base Metal and Heat Affected Zone after Welding*, PhD Dissertation (Department of Materials Science and Engineering, Norwegian University of Science and Technology, Trondheim, Norway, 2012).
- [26] Dr. Mohammad, R. Allazadeh // white paper steel-grips.com (2015) [<http://steel-grips.com/articles/2015/sg15006.pdf>]
- [27] M.S. Rashid, In: *Society Automotive Engineers Congress* (Detroit, 1977).
- [28] M.S. Rashid, E.B. Cpeek, In: *Metallic Materials ASTM STP 647. American Society for Testing and Materials* (Philadelphia, 1978), p.174.
- [29] T. Gladman, *The physical metallurgy of microalloyed steels* (The Institute of Materials, The University Press, Cambridge, London, 1997).
- [30] N.K. Balliger, In: *Advances in the Physical Metallurgy and Applications of Steels*, Book 284 (The Metals Society London, 1982).
- [31] D.L. Steinbrunner, G. Krauss // *Metallurgical Transactions A* **9** (1988) 579.
- [32] S. Kang, H. Kwon // *Metallurgical Transactions A* **18** (1987) 1587.
- [33] M. Azuma, *Structural control of void formation in dual phase steels*, PhD Dissertation (Department of Wind Energy, Technical University of Denmark, Denmark, 2013).